Supplementary Information

Spin coupling and relaxation inside molecule-metal contacts

Aitor Mugarza[1,2*], Cornelius Krull[1,2], Roberto Robles[2], Sebastian Stepanow[1,2], Gustavo Ceballos[1,2], Pietro Gambardella[1,2,3]

[1] *Catalan Institute of Nanotechnology (ICN), UAB Campus, E-08193 Barcelona, Spain*

[2] *Centre d'Investigacions en Nanociència i Nanotecnologia (CIN2), UAB Campus, E-08193 Barcelona, Spain*

[3] *Institució Catalana de Recerca i Estudis Avançats (ICREA) and Departament de Física, Universitat Autonoma de Barcelona, E-08193 Barcelona, Spain*

Supplementary Figures

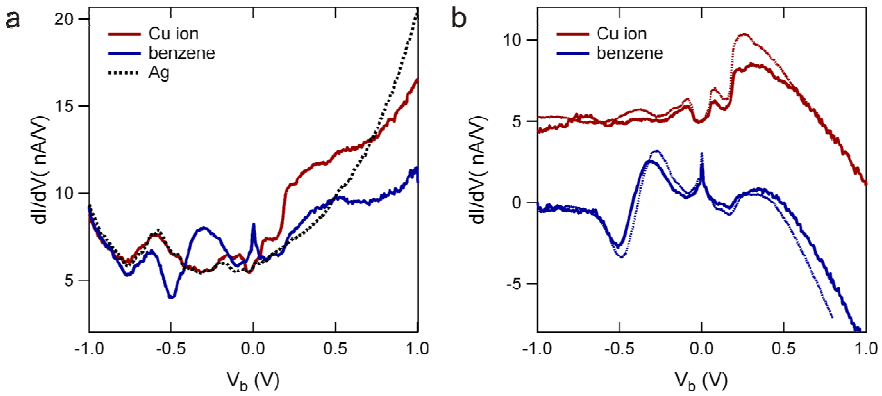

Supplementary Figure S1: Ag background subtraction procedure. *(**a**) dI/dV spectra acquired on the Cu ion (red), and benzene (blue) of a single CuPc molecule, and on the Ag surface (dotted black) (initial setpoint: I = 3.0 nA, V_b = -1.0 V). (**b**) The same ion and benzene spectra after subtraction of the Ag spectrum (thick solid lines). For comparison, we show a pair of background subtracted spectra (thin dotted lines) acquired with a different tip and initial setpoint (I = 3.0 nA, V_b = -2.0 V). The intensity of the latter have been reduced by a factor of 0.5 to account for the different initial setpoint. The spectra recorded on the Cu ion have been vertically shifted by 5 nA/V for better visibility.*

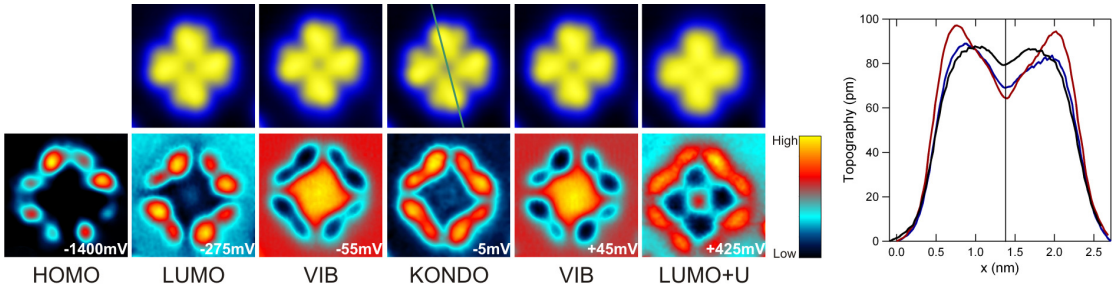

Supplementary Figure S2: *dI/dV maps of the molecular orbitals of a single CuPc displayed in Fig. 1 of the main text, together with the topographic signal simultaneously obtained at each energy. The map at -5 mV shows the intensity distribution of the* d^2I/dV^2 *signal, following the method explained in this section. Topographic profiles across the molecule (line on the topography recorded at -5 mV) for images taken at -275 mV (blue), -5 mV (red), and +425 mV(black) are displayed on the right.*

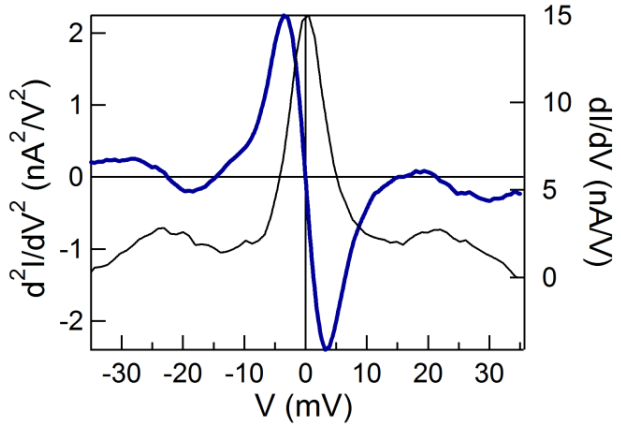

Supplementary Figure S3: *Comparison between first (black) and second derivative (blue) of a CuPc spectrum showing a Kondo resonance. The maximum of the second derivative at negative voltage is used to map the Kondo resonance.*

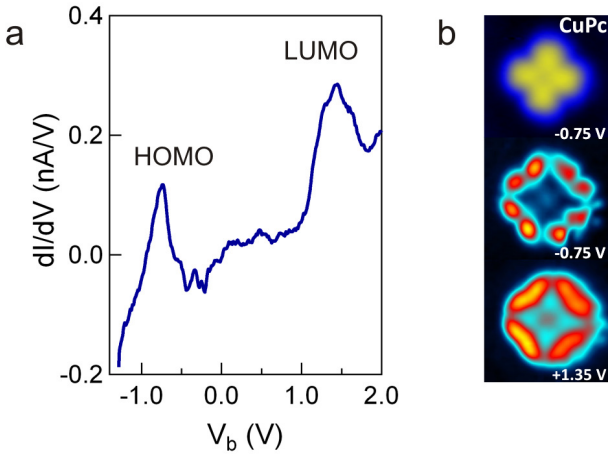

Supplementary Figure S4: Electronic structure of CuPc on Au(111). *(**a**) dI/dV spectra of a single CuPc on Au(111) acquired at the benzene position. A spectrum acquired on the bare Au surface has been subtracted to enhance the molecular features (initial setpoint : I = 0.25 nA, V_b = -1.3 V). (**b**) Topography and dI/dV maps of the HOMO and LUMO.*

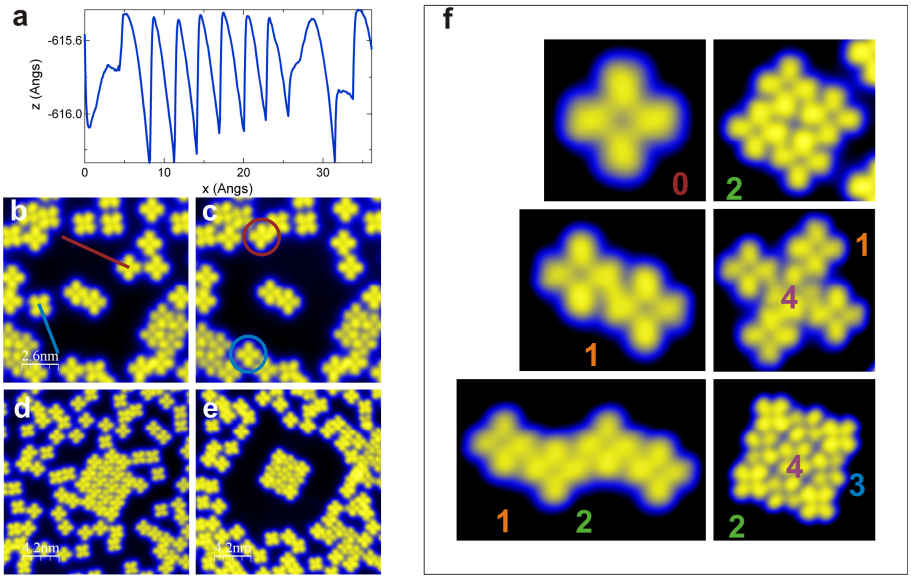

Supplementary Figure S5: Lateral manipulation of CuPc molecules. *(**b**) and (**c**) Images before and after dragging two molecules. A gap resistance of 333 KΩ was used for manipulation, and 74 MΩ for imaging. The tip height variation during the manipulation of one of them is shown in **a** (blue line in **b**). (**d**) and (**e**) Images before and after the formation of a 3x3 square cluster. (**f**) Examples of CuPc clusters used in the study of the dependence of the Kondo interaction on the number of intermolecular bonds. The number of lateral bonds of different molecules is indicated.*

Supplementary Tables

E_{exp} (meV)	E_{th} (meV)	Symmetry	Int	Active
5.9	7.7	$1E_g$	0.15	R
18.5	13.6	$1B_{2g}$	11.69	R
	14.9	$2E_g$	12.93	R
	20.7	$1B_{1g}$	18.03	R
	25.6	$1A_{2g}$	0	R
29.4	28.5	$2B_{2g}$	30.8	R
	29.8	$3E_g$	6.56	R
	31.0	$1A_{1g}$	71.2	R
	33.9	$4E_g$	0.77	R
48.8	52.1	$5E_g$	0.01	R
55.9	58.7	$3B_{2g}$	97.63	R
	59.9	$6E_g$	1.31	R
	67.7	$2B_{1g}$	0.67	R
	70.2	$2A_{2g}$	0	R
72.5	72.0	$2A_{1g}$	72.8	R
	75.8	$3A_{2g}$	0	R
	76.8	$7E_g$	1.81	R
83.9	82.9	$3A_{1g}$	298.93	R
	83.6	$4B_{2g}$	6.04	R
	86.2	$8E_g$	21.03	R
93.3	91.2	$3B_{1g}$	822.17	R
	93.7	$9E_g$	0.14	R
	94.2	$10E_g$	5.17	R

Supplementary Table 1*: Computed Raman vibrational energies (from Ref. 21). The experimental values of the vibrational modes obtained from the fit of the differential conductance spectra (example shown in Fig. 1c of the main text) are listed on the left column.*

	ΔN (electrons)	m (μ_B)
CuPc	1.24	0.91
NiPc	1.07	0.00

Supplementary Table 2*: Charge transfer (ΔN) and magnetic moment (m) computed for CuPc and NiPc on Ag(100). The latter does not include the LUMO spin.*

Supplementary Methods

I. Background subtraction

A spectrum acquired on the bare Ag surface with the same feedback conditions has been subtracted to all spectra reported in the paper in order to remove electronic features due to the substrate and tip. This simple background subtraction method is reliable as long as the reference spectra do not present sharp features[46], which was routinely confirmed in all our experiments. As an example, Supplementary Fig. S1 displays a set of spectra taken on the Cu ion and benzene of a single CuPc before and after subtraction of the spectra recorded on the bare Ag substrate. Comparing background subtracted spectra obtained using different tips (Supplementary Fig. S1b), we see that this procedure yields reproducible spectra. Moreover, the strong, tip-related feature appearing around 0.6 V in the Ag spectrum of Supplementary Fig. S1a is basically removed, showing the efficacy of this method. Note that, due to this subtraction, the conductance values reported for the spectra represent relative values, negative values only meaning that conductance at the molecule at a certain energy is lower than that of the substrate.

II. Spectroscopic maps

Spectroscopic maps were obtained while scanning at constant current with closed feedback loop. In principle, the convolution of topographic and spectroscopic information may complicate the proper identification of molecular orbitals in the *dI/dV* maps. However, our measurements indicate that intramolecular changes of height profile are relatively small, as shown by the linecuts in Supplementary Fig. S2. This occurs due to the additional contribution of the vibrational channels, which have strong intensity at the center of the molecule and compensate for the small overlap of tip and mo-

lecular orbitals in this region. Thus, convolution effects between topographic and spectroscopic features inside the molecules are expected to be small. Moreover, topographic maps of the same molecule recorded at different energies (top row, Supplementary Fig. S2) do not show strong variations of the molecule profile. This allows us to compare the spectroscopic maps recorded at different energies and, specifically, to relate the similar appearance of the maps taken at -275 mV and +425 mV to a single molecular orbital, i.e., the LUMO, and the latter with the Kondo resonance.

Since zero bias resonances cannot be measured with closed feedback, we have mapped the conductance near E_F by measuring the second derivative of the current, mapping either the maximum or the minimum of the d^2I/dV^2 signal, which are slightly offset from $V_b = 0$, as shown in Supplementary Fig. S3. The validity of this approach is justified by the fact that, for a Lorentzian function, the intensity maximum of the peak is proportional to the (shifted) maximum of its derivative. The Kondo resonances measured in our experiment correspond to Fano functions with a high q value (see Sec. IV of Supplementary Discussion), i.e., to Lorentzian functions within a very good degree of approximation.

Finally, we remark that the conductance spectra and maps of CuPc and NiPc reported in this work are entirely reproducible, that is, they do not vary from molecule to molecule.

Supplementary Notes

Supplementary Note 1. Analysis of the inelastic excitations

The conductance spectra acquired on Cu and Ni ions display multiple inelastic excitations, as shown in Fig. 1 of the main text. These inelastic features can be better distinguished by measuring the second derivative (d^2I/dV^2) of the tunneling current (see Fig. 1d). We analyzed the energies at which the inelastic conductance steps and corre-

lated Kondo peaks occur (labeled as K_{v1}-K_{v8} in Fig. 1c), and compared them to vibrational modes calculated for CuPc in the gas-phase[21]. Raman active modes are the ones with highest intensity in the d^2I/dV^2 spectra due to their symmetrical character with respect to the σ_v planes of the molecule. According to symmetry selection rules, such modes are the only ones that present maximum intensity at the mirror planes of the molecule when the electronic orbitals involved in the inelastic process are symmetrical[39]. This is the case of the b_{1g} and $2e_g$ states. In Supplementary Table I we compare the experimental vibrational energy values with the calculated Raman modes for CuPc. The agreement between the experimental values and the Raman modes is very satisfactory. The fact that the spectra taken at the metal position in both CuPc and NiPc present identical inelastic structure and their close correlation with calculated vibrational modes demonstrates that the origin of the non-equilibrium Kondo resonances K_{v1}-K_{v8} is indeed vibrational. We note that the exact correspondence of the NiPc and CuPc vibrational modes found in the experiment excludes the possibility of assigning the CuPc Kondo sidebands at $E_{Kts} = \pm 21$ meV to nonequilibrium vibrational processes. Moreover, the presence (absence) of a local spin on Cu (Ni) points univocally to an inelastic triplet-singlet excitation. The possibility for such metal-ligand exchange interaction in CuPc is demonstrated by DFT calculations of the magnetic structure of the gas-phase anion, as explained in the main text. Interestingly, the magnitude of the intramolecular exchange coupling J is similar to that estimated for carrier-mediated exchange between stacked CuH_2PcI molecules in bulk crystals, where the itinerant spin is thought to arise from a I-induced hole in the HOMO[47].

The large increase in conductance observed for the vibrational features, up to 5-10%, indicates that tunneling occurs through an orbital that is strongly coupled to the CuPc and NiPc vibrational modes but has weak coupling to the substrate[48]. The d_{x2-y2} orbital fulfills these conditions as all the observed vibrational modes involve a distortion

of the Cu-N bonds, where the d_{x2-y2} state has most of its weight and strong electron-phonon coupling.

The energy, intensity and width of the conductance steps and Kondo cusps have been analyzed by fitting the data with step and Lorentzian functions, respectively, as shown in Fig. 1c of the main text. The use of Lorentzians instead of Fano functions for the Kondo resonances is justified by the large q factor obtained using the latter (see Section IV). Symmetry considerations considerably reduce the number of free parameters in the fit. The inflection point of the step functions and the Lorentzian peaks were fixed to the same values, symmetric with respect to E_F. This is justified since the energy of the nonequilibrium cotunneling events necessarily coincides with that of the vibrational modes. The step width was kept constant at all energies, whereas the width of the Lorentzian peaks was allowed to vary. As shown in Fig. 1c, we distinguish up to eight different vibrational excitations K_{v1}-K_{v8}. However, only peaks that stand out with enough intensity to give reproducible results for different initial values of the fit parameters were retained for the analysis presented in Fig. 6b of the main text, namely peaks K_{v4}-K_{v6} for NiPc and K_{v5}-K_{v6} for CuPc. The error bars reported in Fig. 6b represent the standard deviation of Γ/Γ_K obtained in a series of 8 fits using different initial parameters for the intensity and broadening of each vibrational feature.

Supplementary Note 2. Ab-initio electronic structure calculations

Relative to the gas-phase molecules, the main difference of the electronic structure of CuPc and NiPc adsorbed on Ag(100) concerns the LUMO. This is a doubly degenerate $2e_g$ (π^*) orbital localized around the aromatic Pc ring, which fills by approximately one electron due to charge transfer from the substrate (see Supplementary Table II). The electronic structure of the aromatic ring is similar in both molecules (Fig. 3a of the main text), in agreement with the experimental findings. The partial filling of the $2e_g$

state is consistent with the experimental observation of a Kondo-screened magnetic moment delocalized over the LUMO orbital, as reported in the main text. Note, however, that the double-peak structure of the LUMO due to the Coulomb repulsion term and, hence, the ligand spin polarization cannot be reproduced by the calculations due to the underestimation of correlation effects typical of DFT[49]. However, in the gas-phase calculation, since non-integer occupations are not allowed, the extra electron of the anion has to go to one of the doubly degenerate $2e_g$ orbitals, coupling parallel (S=1) or antiparallel (S=0) to the existing b_{1g} spin.

We find that the *d*-state occupation of the Cu and Ni ions does not differ significantly from that of the gas-phase, in agreement with recent x-ray magnetic dichroism measurements[12] and contrary to the case of MnPc, FePc, and CoPc[15-18]. The spin polarized density of states projected onto the Cu and Ni *d*-orbitals shows that d_{x2-y2} is the highest energy level, separated by about 2 eV from the remaining orbitals, which form a 2 eV-wide band-like structure (see Fig. 3a of the main text). In the case of CuPc, the d_{x2-y2} level is partially occupied with 1 electron, leading to a d^9configuration and S = 1/2[12], as reflected by the computed magnetic moment displayed in Supplementary Table II. On the other hand, the Ni^{2+} ion in NiPc has one electron less and is in a d^8 configuration with S=0. The similarities between gas-phase and adsorbate results indicate that there is no significant charge transfer into the *d*-states and that changes of the crystal field upon adsorption are negligibly small, as expected for an undistorted adsorption configuration and verified also by x-ray absorption spectroscopy[12].

Supplementary Note 3. Electronic structure of CuPc on Au(111)

In order to study the amount of charge transfer for different substrates, we performed spectroscopic measurements of single CuPc on the Au(111) surface. Compared to Ag(100), this surface is less reactive because of the larger noble-metal character of

Au as well as the tighther close-packed structure of the (111) plane. The *dI/dV* spectra and maps shown in Supplementary Fig. S4 show the HOMO resonance at -0.75 eV and a single LUMO feature at about 1.4 eV, implying a much reduced charge transfer for this surface. The LUMO thus remains unfilled as in the gas-phase, consistently with the fact that no Kondo resonance is observed for this system.

Supplementary Note 4. Temperature dependence of the zero bias Kondo peak

The temperature dependence of the zero-bias Kondo resonance of CuPc was analyzed by raising the temperature of the Ag substrate from 4.8 to 35 K. Temperature dependent *dI/dV* spectra measured at the benzyne ring position were fitted with Fano functions, with q values varying from 120 to 60 for increasing temperature. As the difference between Fano and Lorentzian functions is practically negligible for such large q values, the use of Lorentzian functions to fit the non-equilibrium Kondo resonances at finite bias is justified in the case of vibrational as well as spin excitations.

Figure 2c of the main text shows that the zero bias (Γ_K) and triplet-singlet resonance (Γ_{ts}) lifetimes of CuPc split off at low temperature and saturate at different values. This is attributed to the contribution of inelastic excitations in Γ_{ts}, which increase the relaxation rate. The intensity of both zero bias and triplet-singlet resonances shown in Fig. 2b, on the other hand, follows the same logarithmic decrease in the whole temperature range studied in this work, thus confirming the Kondo origin of the side peaks. The intensity of the zero bias resonance was fitted with expressions obtained by numeric renormalization group theory (NRG) for both S=1/2 and S=1,

$$G_s(T) = G_{off} + G(0) \cdot \left[1 + \left(\frac{T}{T_K} \right)^{\xi} \cdot \left(2^{1/\alpha} - 1 \right) \right]^{-\alpha}$$

where (α,ξ) are (0.22,2) for S=1/2, and (0.506,0.745) for S=1[3]. T_K was set to 27 K, according to the fit of $\Gamma_K(T)$ in Fig. 2c. The offset parameter included in G_{off} differs from that used in Ref. 3 due to the different contributions from the background and zero bias conductance, which in STM originate from direct tunneling to the substrate through strongly hybridized molecular states[50]. Note that the small temperature range of the experimental data, which falls in the logarithmic region of the functions, does not allow us to discriminate between the S=1/2 and S=1 models. However, the assignment of S=1 for CuPc as opposed to S=1/2 for NiPc is robust due to the appearance of triplet-singlet excitations, independent measurements of the Cu spin[12], and the results of DFT calculations.

Supplementary Note 5. Molecule manipulation and intermolecular interactions

Tip induced lateral manipulation was used to create artificial molecular clusters of the desired geometry in a controlled and reproducible fashion. The molecules were dragged by the STM tip by reducing the sample-tip distance in order to have gap resistances that varied from 100 to 500 KΩ once the tip was positioned on top of the selected molecule, and laterally moving the tip to the desired place at a speed of 0.5-3 nm/sec. The bias voltage was kept low during the manipulation (< ± 50 mV) in order to minimize excitations of vibrational modes that reduce the degree of control and reproducibility of the manipulation process. We ensured that the molecules remained unperturbed and in the same adsorption configuration after manipulation by comparing topographic images and conductance spectra before and after their displacement. Supplementary Figs. S5b and c report an example of the manipulation of two molecules. The height variation of the tip during one of the manipulation events is shown in Supplementary Fig. S5a, where discrete jumps due to the surface atomic corrugation are clearly visible. Supplementary Figs. S5d and e show images before and after creating a 3x3 “sudoku” cluster. Supplementary Fig. S5f reports images of other molecular clusters studied in the

present work. Note that the conductance spectra and Kondo temperature only depend on the number of lateral bonds of each molecule, and are independent of the overall cluster shape or size.

Supplementary References

46 Wahl, P., Diekhoner, L., Schneider, M. A. & Kern, K. Background removal in scanning tunneling spectroscopy of single atoms and molecules on metal surfaces. *Rev. Sci. Instrum.* **79**, 043104-043104 (2008).

47 Martin, I. & Phillips, P. Exchange coupling and high-temperature transport in M(phthalocyanine)I conductors. *Phy.s Rev. B* **60**, 530-532 (1999).

48 Lorente, N. & Persson, M. Theory of Single Molecule Vibrational Spectroscopy and Microscopy. *Phys. Rev. Lett.* **85**, 2997-3000 (2000).

49 Cohen, A. J., Mori-Sánchez, P. & Yang, W. Insights into Current Limitations of Density Functional Theory. *Science* **321**, 792-794 (2008).

50 Pustilnik, M. & Glazman, L. I. Kondo Effect in Real Quantum Dots. *Phys. Rev. Lett.* **87**, 216601 (2001).